



Optimization of hot-wire fraction for enhance quality in GMAW

N. Suwannatee^{1,2} · M. Yamamoto¹ · S. Shinohara³

Received: 26 July 2023 / Accepted: 2 November 2023 / Published online: 22 November 2023
© International Institute of Welding 2023

Abstract

The combination of hot-wire insertion technology and gas metal arc welding (GMAW) is proposed to enhance the deposition rates while reducing energy consumption. This study systematically investigated the effect of hot-wire fraction on weld metal properties. The results reveal that the compensatory deposition rate from hot-wire insertion provides a similar effective height compared with conventional GMAW, with a lower weld height/width ratio, lower power consumption, and improved mechanical properties. However, an excessive hot-wire fraction may lead to lack of fusion, and this value should be limited to no more than 44% of the total deposition rate. By strategically optimizing the ratios of GMAW and hot-wire fractions, it becomes possible to maximize deposition volume while preventing fusion deficiencies and ensuring adequate penetration. Under these optimized conditions, hot-wire GMAW proves to be an efficient method for achieving equivalent deposition rates with reduced energy consumption and without compromising toughness properties. An electron backscattering diffraction (EBSD) analysis underscores the effectiveness of the proposed approach, particularly when utilizing a 41.16% hot-wire fraction, ensuring both sound joint formation and the predominance of an acicular ferrite microstructure, thereby enhancing mechanical properties. This innovative process presents a sustainable alternative to conventional GMAW, offering substantial benefits of welding technology.

Keywords Hot-wire fraction · Gas metal arc welding · Weld metal properties · Power consumption · EBSD

1 Introduction

The shipbuilding industry faces the challenge of high heat input during welding processes, particularly with conventional methods like submerged arc welding (SAW) [1–4] and electrogas arc welding (EGW) [5–7]. To mitigate this issue and improve weld quality, various welding techniques

and processes have been suggested, including laser beam welding (LBW) [8, 9] and electron beam welding (EBW) [10, 11]. However, these processes have limitations, such as expensive equipment, complex setup, and limited deposition volume. To address these limitations, researchers have explored the amalgamation of arc welding techniques, resulting in processes like laser gas metal arc welding (GMAW) [12, 13] and hybrid laser SAW [14, 15]. While these techniques increase penetration depth, the tolerance for deposited volume is still bounded by the filler metal's burn-off rate. Multiple wire arc processes, such as integrated cold wire SAW [16] and twin-arc integrated cold-wire hybrid welding [17, 18], have been introduced to increase deposition rates without raising heat input by employing a non-arc electrode (cold wire) for augmenting deposition. However, these processes encountered limitations when the cold wire feeding speed exceeded 2.6 m/min. In response, researchers have proposed a solution involving additional volume provided independently of the primary heat source through hot-wire insertion.

The utilization of hot-wire technology was initially conceived to enhance deposition in gas tungsten arc welding

Recommended for publication by Commission XV - Design, Analysis, and Fabrication of Welded Structures

✉ N. Suwannatee
s.nattazak@gmail.com

M. Yamamoto
motoyama@hiroshima-u.ac.jp

S. Shinohara
shinichiro.shinohara@tsuneishi.com

¹ Graduate School of Engineering, Hiroshima University, Hiroshima, Japan

² Engineering Services, TUV NORD (Thailand) Limited, Bangkok, Thailand

³ Tsuneishi Shipbuilding Co., Ltd., Hiroshima, Japan

(GTAW) [19]. By heating the filler wire to just below its melting point and directly feeding it into the molten pool, the hot-wire fraction can melt through the heat of the weld pool, resulting in a standalone increase in deposition volume without elevating the primary heat source. To simplify this process, Shinozaki et al. [20] and Zhu et al. [21] introduced equations for different filler metals, establishing a proportional relationship between hot-wire feeding speed and current. The use of hot wire has significantly augmented deposition in conjunction with various welding techniques, including hot-wire LBW [22–24] and hot-wire SAW [25]. Furthermore, Tsuyama et al. [26] introduced the concept of combined hot-wire GMAW, which can match the deposition volume achieved in SAW. Notably, a successful single-pass weld of a 15-mm thick steel butt joint, devoid of edge preparation, was achieved at a travel speed of 0.6 m/min, coupled with 15 m/min of hot-wire feeding speed (equivalent to 18 kg/h of total deposition volume) [27]. Studies conducted by Wonthaisong et al. [28] have concentrated on optimizing the hot-wire fraction, leading to the formation of single-V butt joints in 20-mm thick steel plates. These joints exhibited increased weld metal hardness, although detailed insights into the weld metal microstructure were not provided. Nonetheless, the application of hot-wire technology has revealed certain limitations, including the potential for excessive deposition volume from the hot-wire and GMAW filler metals, which may manifest as irregular bead shapes, incomplete fusion, and precedence of molten metal [29].

This study investigated the impact of hot-wire fraction on the properties of weld metal in hot-wire GMAW. The investigation was planned and conducted in three stages. In the first stage, the compensatory condition was studied, where a hot wire was used to increase the deposition rate while minimizing the GMAW fraction, and was compared with similar deposition rates using only the GMAW condition. The second stage determined the maximum hot-wire fraction that could be used without causing welding defects or detrimental effects on weld metal properties. In the third stage, the fractions of hot wire and GMAW were optimized at the highest deposition rate to achieve a sound joint with the lowest energy consumption. This systematic approach showed that the hot-wire GMAW process offers a sustainable alternative to conventional GMAW.

2 Experimental procedure

A single-V butt joint was configured using K36E-TM (490 MPa-class) as a base material and backing plate. A groove angle of 30° with a root gap of 4 mm was employed, as shown in Fig. 1. A solid wire of G49A0UC11 (JIS Z3312 YGW11) with a diameter of 1.2 mm was used for both

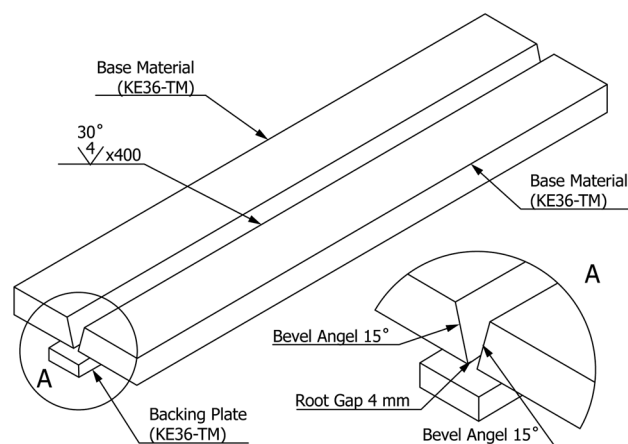


Fig. 1 Joint configuration

GMAW and hot-wire filler metals. The chemical compositions of materials used in this work can be found in Table 1.

The experiment setup is illustrated in Fig. 2, where the hot-wire torch was positioned 10 mm behind the GMAW torch in the welding direction. To establish the baseline conditions, the GMAW process was conducted alone using a constant deposition rate of 114.95 g/min (equivalent to a welding current of 300 A) on the root pass for all conditions. The investigation was conducted in three stages. Each set of welding parameters was subjected to five repetitions.

In the first stage, the GMAW process was performed alone using deposition rates of 180.12 and 193.70 g/min (equivalent to welding currents of 400 A and 500 A, respectively) on the second pass to establish two master conditions, referred to as condition 1 (Master A) and condition 2 (Master B). The next step involved using the hot-wire insertion technique to increase the deposition rate while minimizing the GMAW fraction. A compensatory condition was achieved by maintaining a constant deposition rate of GMAW at 114.95 g/min (equivalent to welding currents of 300 A), with hot-wire insertion requiring deposition rates of 65.17 and 78.75 g/min for the compensatory condition, referred to as condition 3 (Compensation A) and condition 4 (Compensation B), respectively. To achieve an accurate deposition rate, the hot-wire current was calculated using a simplified equation [20, 21], which clarifies the dependence of hot-wire current on wire feeding speed.

In the second stage, while maintaining the GMAW deposition rate at 114.95 g/min (equivalent to welding currents of 300A), the hot-wire deposition rate was systematically increased from 90.51 g/min (equivalent to wire feeding speed of 10 m/min) up to a maximum of 135.57 g/min (equivalent to wire feeding speed of 15 m/min). These conditions were applied on the second pass, completing a full single-V joint within two weld passes. This enabled the determination of the limiting hot-wire fraction without

Table 1 Chemical composition of materials used in this experiment

Chemical composition (%wt)	C	Si	Mn	P	S	Cu	Ni	Cr	Ti+Zr	Fe
K36E-TM	0.12	0.20	1.20	0.14	0.04	0.01	0.01	0.02	-	Bal
G49A0UC11	0.08	0.51	1.10	0.01	0.01	-	-	-	0.05	Bal

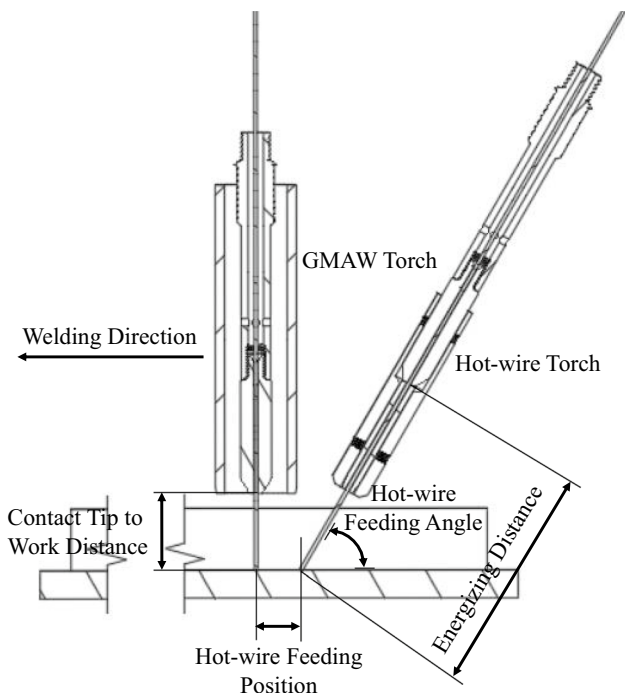


Fig. 2 Schematic illustration of hot-wire gas metal arc welding

causing defects or detrimental effects on weld metal properties. In the third stage, the hot-wire and GMAW fractions were optimized to achieve the highest total deposition rate of 250.72 g/min while maintaining a sound joint with minimal energy consumption.

Table 2 provides the hot-wire fractions under welding conditions for all three stages of the experiments. The hot-wire fraction, expressed as a percentage of the total deposition rate, was determined using Eq. 1:

$$\%HW = [V_{HW} / (V_{HW} + V_{GMAW})] \times 100 \tag{1}$$

where %HW is the hot-wire fraction of total deposition, in %; V_{GMAW} is the deposition rate of GMAW, in g/min; and V_{HW} is the deposition rate of hot-wire insertion, in g/min.

To isolate the effect of the hot-wire fraction, the welding and related parameters were held constant, as shown in Table 3.

Molten pool formation and arc phenomena were observed in detail using a MEMRECAM HX-7 high-speed camera with an 810 ± 10 nm band-pass filter. The captured

condition had a resolution of 500 fps, and the shutter speed was 1/1000 s. The temperature of the molten pool was measured using an R-type contact thermocouple that was directly placed in the molten pool during welding. The actual current and voltage of both the GMAW and hot wire were determined at 5 kHz intervals using a data acquisition system. Power consumption was calculated using Eq. 2:

$$P_{GMAW} = [(I_{w1} \times V_{w1}) + \dots + (I_{wn} \times V_{wn})] / n, \tag{2}$$

where P_{GMAW} is the power consumption of GMAW, in W; I_w is the welding current, in A; V_w is the arc voltage, in V; n is the number of samples; and,

$$P_{HW} = [(I_{h1} \times V_{h1}) + \dots + (I_{hn} \times V_{hn})] / n, \tag{3}$$

where the symbols have the analogous values for the hot wire. Then,

$$P_{total} = [(P_{GMAW} + P_{HW}) \times t] / 1000, \tag{4}$$

where P_{total} is total power consumption, in kJ; t is welding time, in s. This value is used to justify the optimized welding conditions.

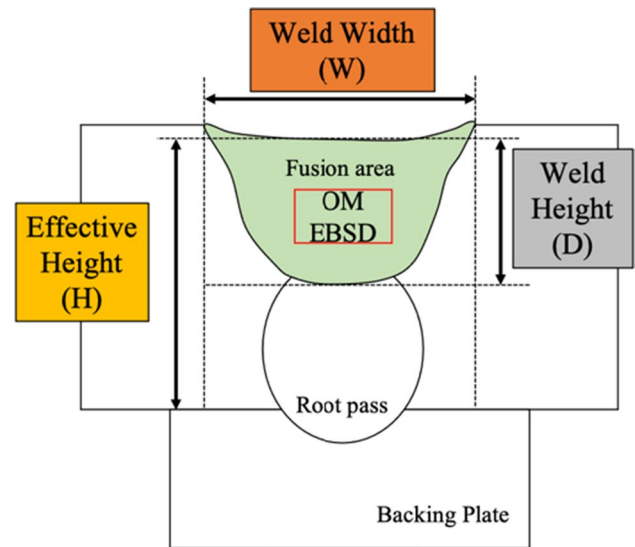
Cross-sectional specimens were prepared for microstructure observation. Mechanical polishing was conducted using abrasive papers ranging from 80 to 2000 grits, followed by a final polishing step with a diamond suspension. The prepared surfaces were treated with a 2% nitric acid solution and then observed at the center of the weld metal area through optical microscopy (OM), as represented by the red square in Fig. 3. For EBSD observations, specimens were polished using the same method as OM, with an additional polishing step using a 0.04 μ m OPS suspension. SEM imaging was carried out at 15 kV with a step size of 0.5 μ m. Geometric parameters of the weld profile, such as fusion area, effective height (H), weld width (W), and weld height (D), were measured to calculate the D/W ratio. Vickers hardness tests were performed according to ISO 6507–1:2023 on the etched surface of the weld metal area with a load of 10 kgf (HV10). Charpy impact test specimens were prepared with a thickness and width of 10 mm perpendicular to the welding direction, in accordance with ISO 148–1:2006. The absorbed energy was determined at a hammer speed of 5.5 m/s and a temperature of 0 °C, maintained by liquid nitrogen (with a maximum testing machine capacity of 300 J).

Table 2 Welding conditions

Parameters/process(es)	GMAW	GMAW	HW GMAW	HW GMAW	HW GMAW	HW GMAW	HW GMAW	HW GMAW	HW GMAW	HW GMAW
Hot-wire current, A	-	188	205	218	241	262	232	195		
Wire feeding speed, m/min	-	7.20	8.70	10.00	12.50	15.00	11.40	7.80		
Deposition rate, g/min	-	65.17	78.75	90.51	113.14	135.57	103.19	70.60		
Welding current, A	400	500	300	300	300	300	350	400		
Wire feeding speed, m/min	19.90	21.40	12.70	12.70	12.70	12.70	16.30	19.90		
Deposition rate, g/min	180.12	193.70	114.95	114.95	114.95	114.95	147.54	180.12		
Total deposition rate, g/min	180.12	193.70	193.70	205.47	228.10	250.72	250.72	250.72		
Hot-wire fraction, %HW	0	0	40.65	44.05	49.60	54.15	41.16	28.16		
Total energy input, kJ/mm	3.04	3.80	2.32	2.32	2.33	2.33	2.70	3.08		
Condition No	1	2	3	4	5	6	7	8	9	

Table 3 Constant parameters

Parameters	Value
Arc voltage, V	38
Travel speed, mm/s	5
Contact tip to work distance, mm	25
Energizing distance, mm	100
Hot-wire feeding angle, °	70
(100% CO ₂) Gas flow rate, L/min	25

**Fig. 3** Measured parameters and observation positions

3 Results and discussion

3.1 Compensatory conditions

The high-speed images in Fig. 4 demonstrate the effect of hot-wire fraction on the position and shape of the molten pool during arc welding. As the hot-wire fraction increased, the position of the GMAW filler metal tip shifted upward, leading to a larger accumulation of molten metal at the front of molten pool. Additionally, this shift suppressed penetration of the arc, resulting in a spread of the molten pool to both sides, perpendicular to the welding direction, which yielded a wider bead width. Macroscopic cross-section images of the etched surface further demonstrated changes in the shape and geometry of the weld metal resulting from the application of the hot wire.

By applying the hot wire at a similar total deposition rate as the conventional GMAW process, the molten pool position shifted upward, resulting in a shallower weld depth and wider weld width, as illustrated by the orange and gray bars in Fig. 5. This led to a reduction in the D/W

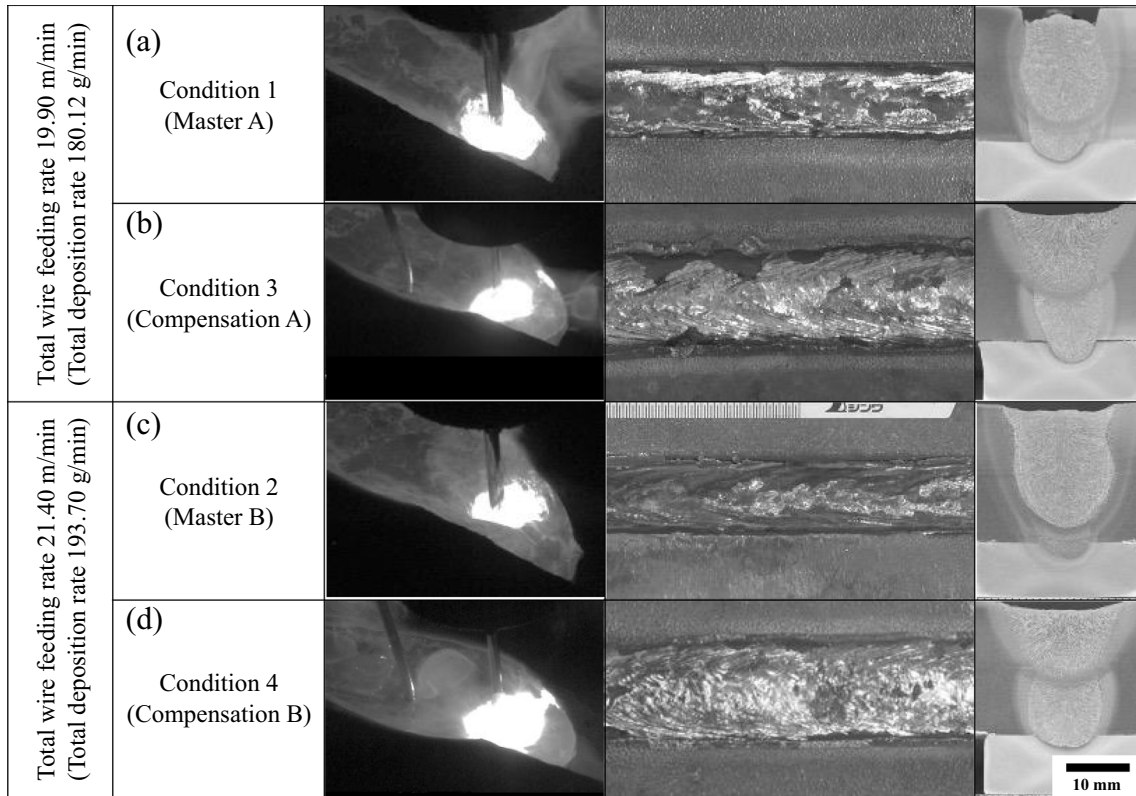
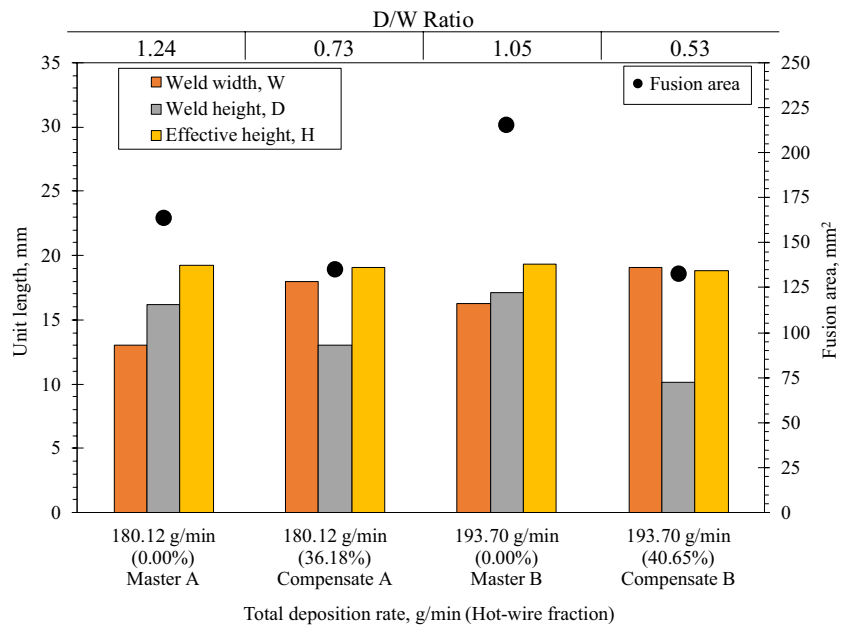


Fig. 4 Captured arc observations, bead appearances, and macroscopic cross-sections of welds for **a** Master A, **b** Compensate A, **c** Master B, and **d** Compensate B

Fig. 5 Weld geometry measurements for compensation stage



ratio and fusion area. However, the yellow bars in Fig. 5 indicate that a similar effective height could be achieved with hot wire at the same deposition rate. A recent study

[27] defined the shallower penetration as a lifting effect when the hot wire was applied. Effects of hot-wire parameters on weld geometry were reported by Tsuyama et al.

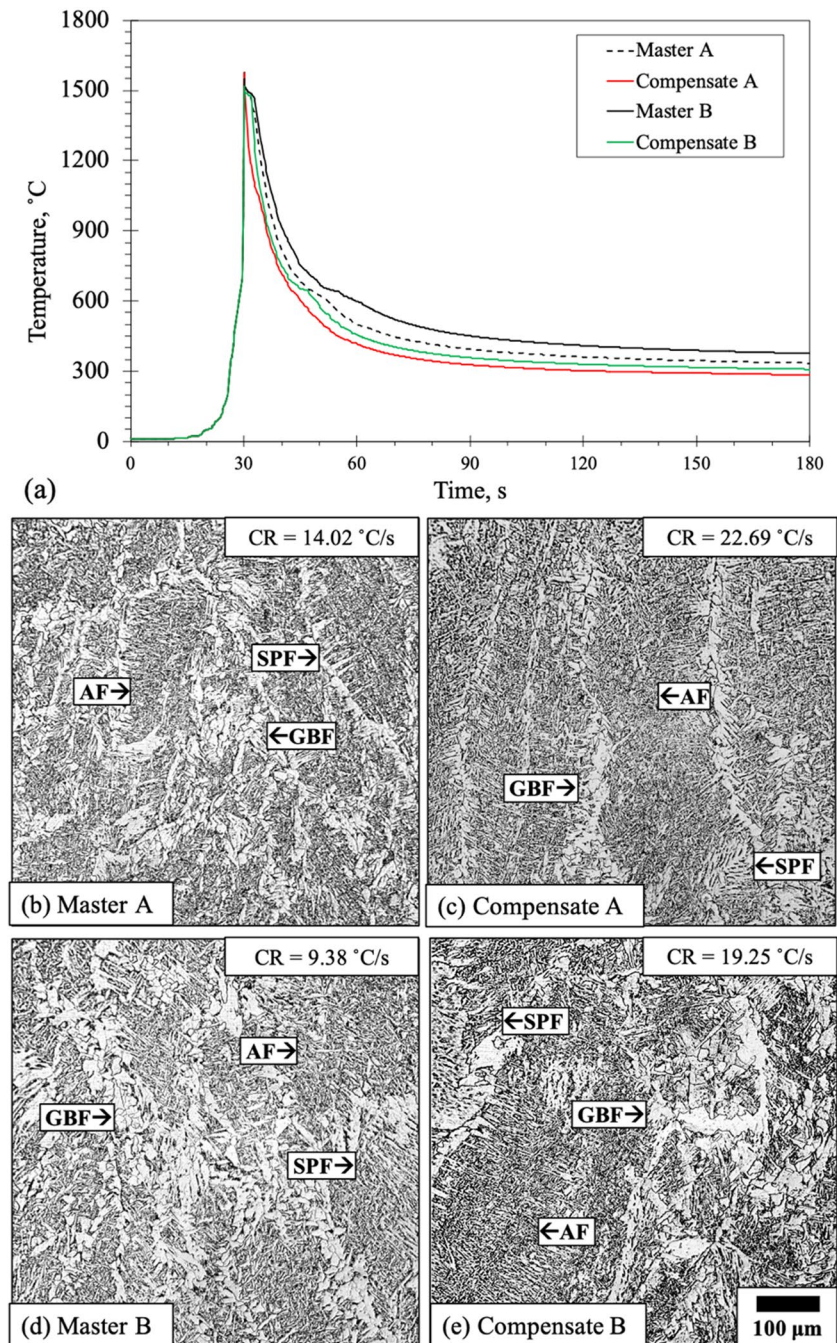
[26] and Wonthaisong et al. [28]. These results suggest that hot-wire insertion can influence the molten pool formation behavior, which in turn affects the geometry of the resulting weld.

Differences in the cooling behavior of weld metals influence their microstructure variations. Both hot-wire application conditions resulted in faster cooling rates compared with the conventional GMAW condition, as illustrated in Fig. 6. Specifically, at a total deposition rate of 180.12 g/min, the cooling rate increased from 14.02 to 22.69 °C/s, while at 193.70 g/min, it increased from 9.38 to 19.25 °C/s.

The faster cooling rates resulted in a lower fraction of grain boundary ferrite (GBF) and side-plate ferrite (SPF), but a higher fraction of acicular ferrite (AF), consistent with previous reports [30–33]. However, at the higher deposition rate of 193.70 g/min, the cooling profile showed an extended delay in the temperature range from 650 to 600 °C as in Fig. 6a, resulting in a higher fraction of GBF [4, 34–37]. As shown in Fig. 6d, the GBF fraction was still enriched, despite the rapid cooling rate under this condition.

At a similar deposition rate, hot-wire insertion resulted in elevated hardness and improved absorb impact energy

Fig. 6 Cooling rates and weld metal microstructures for **a** Master A, **b** Compensation A, **c** Master B, and **d** Compensation B



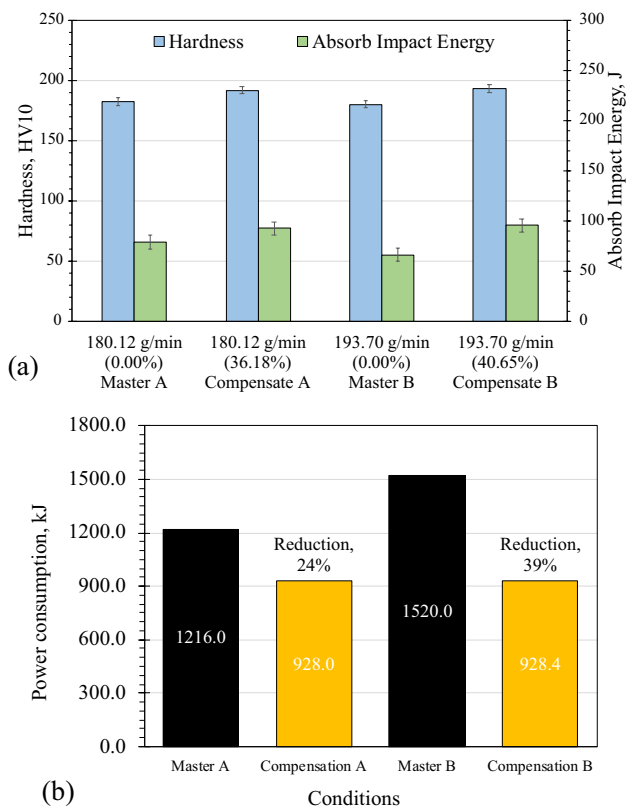


Fig. 7 Effect of compensatory hot-wire fraction on **a** hardness and absorb impact energy and **b** power consumption

of the weld metal, as depicted in Fig. 7a. Specifically, the average hardness values and absorb impact energy increased from 182 ± 5 to 191 ± 10 HV10 and from 65 ± 7 to 77 ± 5 J, respectively, for Master A and Compensation A conditions. Similarly, for Master B and Compensation B conditions, hardness values increased from 180 ± 11 to 193 ± 7 HV10, and absorb impact energy improved from 55 ± 7 to 79 ± 9 J. These enhancements in mechanical properties closely correlate with the microstructure of the weld metal. Nonetheless, when comparing the compensation conditions with hot-wire fractions of 36.18% and 40.65%, no significant differences in mechanical properties were observed. These outcomes indicate that hot-wire insertion can effectively compensate for the total deposition rate while enhancing the mechanical properties of the weld metal. These results suggest that hot-wire insertion can be used to compensate for the total deposition rate and improve the mechanical properties of the weld metal. The compensated fraction allows a similar deposition rate to be obtained with lower power consumption, as shown in Fig. 7b. At 180.12 g/min total deposition rate, the power consumption was reduced by approximately 24%. Additionally, a power saving of up to 39% at 193.70 g/min total deposition rate was recorded, highlighting another advantage of hot-wire insertion. However, it should be noted

that the occurrence of a GBF fraction while applying the hot-wire technique requires further investigation to ensure the obtained weld metal structure while also minimizing power consumption.

3.2 Limitation of hot-wire fraction

To investigate the effects of hot-wire fraction on arc phenomena during welding and on the obtained microstructure, Compensations A and B were included to represent 36.18% and 40.65% of the hot-wire fraction (HW), respectively. Figure 8 shows captured motion during welding with these increased hot-wire fractions while the GMAW fraction was held constant. As the hot-wire fraction increased, the tip of the GMAW filler metal moved upward and the accumulation of molten metal at the molten pool's front became more significant. However, at a hot-wire fraction of 54.15%, the molten pool's front collapsed and advanced ahead of the arc position, resulting in a lower arc position. This phenomenon, known as molten metal precedence, has been reported in the cases of excessive total deposition volume [28, 29]. Notably, the bead appearance under the 54.15% HW condition showed a pronounced humping bead, a clear indicator of molten metal precedence [27–29]. Figure 9 visually demonstrates the sequence of molten metal behavior at a hot-wire fraction of 54.15%. Initially, the molten pool was elevated due to the additional deposit volume from the hot-wire insertion (a). Subsequently, more molten metal accumulated at the front of the molten pool (b). The molten pool front extended and flowed ahead of the arc position (c). Eventually, the raised molten pool collapsed at the front, resulting in a lengthy molten metal precedence, along with a downward shift of the arc (d). Moreover, a lack of fusion was unexpectedly observed at 49.60% HW, where molten metal precedence was not detected by the high-speed camera during hot-wire GMAW, as shown in Fig. 8d.

The influence of hot-wire fraction on cooling behavior was examined, revealing its role in delaying the cooling rate and prolonging the time between temperatures of 650 and 600 °C during solidification. This led to an increased fraction of grain boundary ferrite (GBF) in the fusion zone. The highest hot-wire fraction of 54.15% HW resulted in the slowest cooling rate and the highest GBF fraction. Conversely, applying a lower hot-wire fraction resulted in less GBF fraction. As shown in Fig. 10b and c, a higher acicular ferrite (AF) fraction with a small portion of GBF was observed at 44.05% HW and 49.60% HW, respectively. These findings suggest that the optimal hot-wire fraction should be determined to achieve the desired microstructure and minimize the occurrence of defects.

Figure 11 demonstrates the measured weld geometry at various hot-wire fractions while maintaining a constant

Fig. 8 Captured arc observations and bead appearances for **a** 36.18% HW, **b** 40.65% HW, **c** 44.05% HW, **d** 49.60% HW, and **e** 54.15% HW

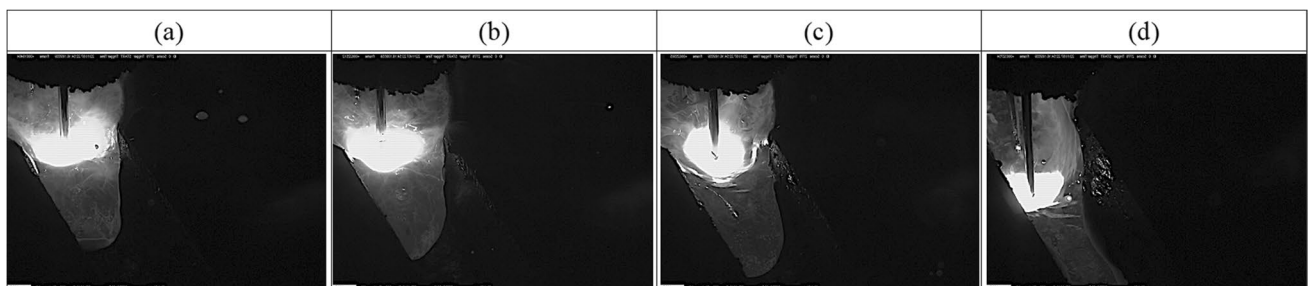
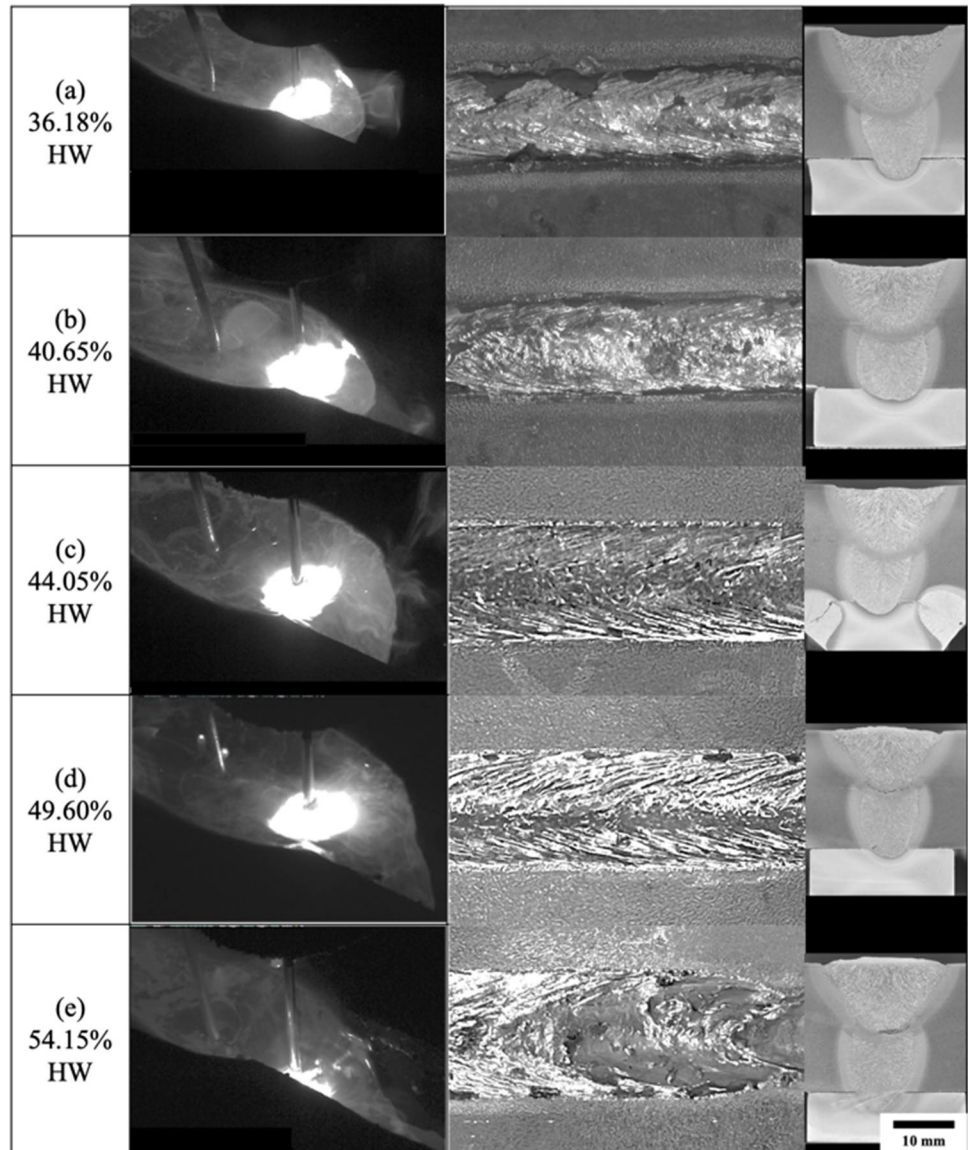


Fig. 9 Molten metal development: **a** molten pool rose, **b** accumulated molten pool front, **c** extended molten pool front, **d** collapsed

GMAW fraction. The yellow bars represent the effective height, indicating that only a hot-wire fraction of 54.15% resulted in weld reinforcement without surface defects.

However, due to incomplete fusion at the interlayer, the precise weld height under these conditions could not be determined. Therefore, the red bars represent the weld

Fig. 10 Cooling rates and weld metal microstructures for **a** 44.05% HW, **b** 49.60% HW, and **c** 54.15% HW

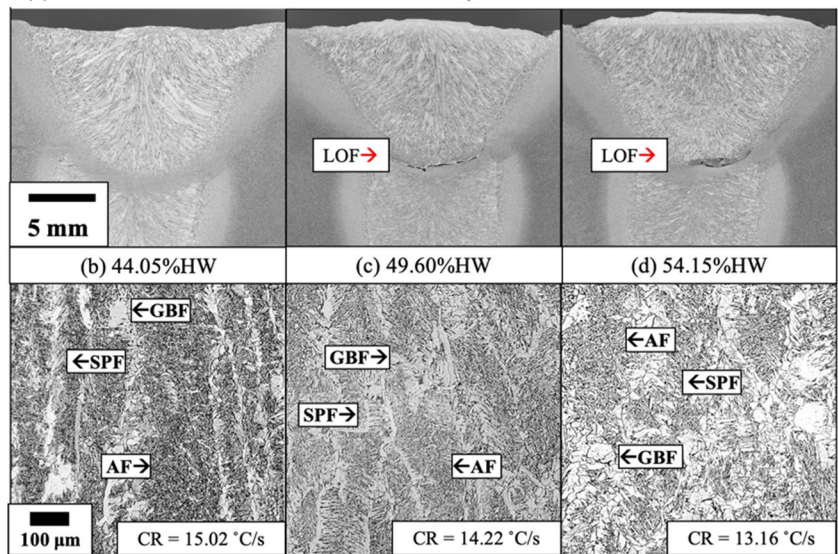
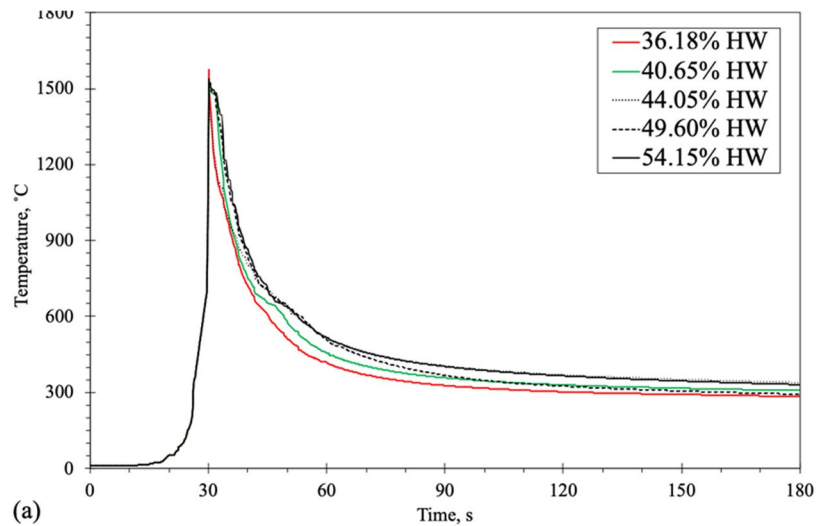


Fig. 11 Weld geometry measurement at hot-wire limitation

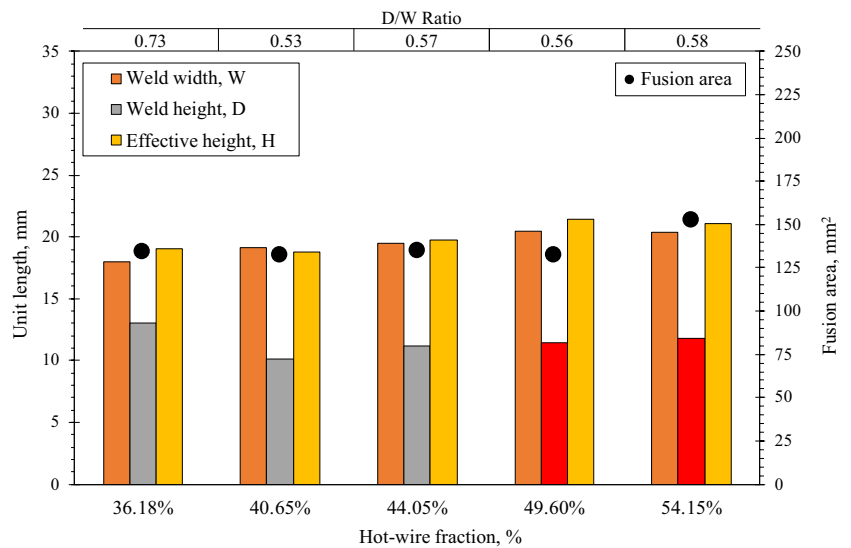
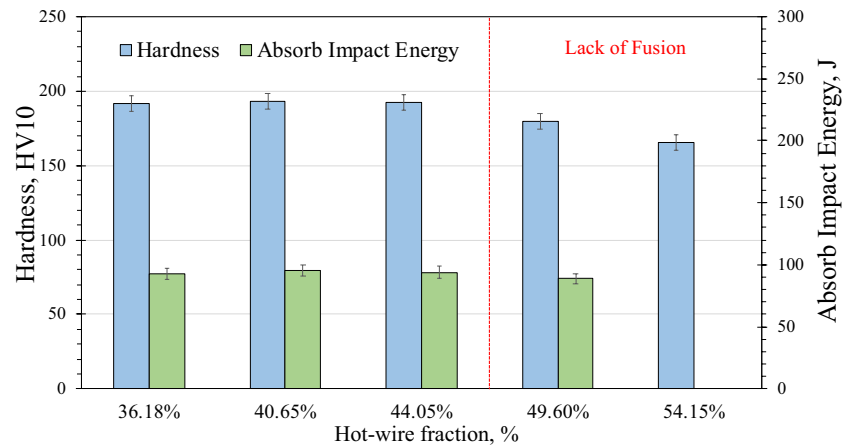


Fig. 12 Hardness and toughness of various hot-wire fractions

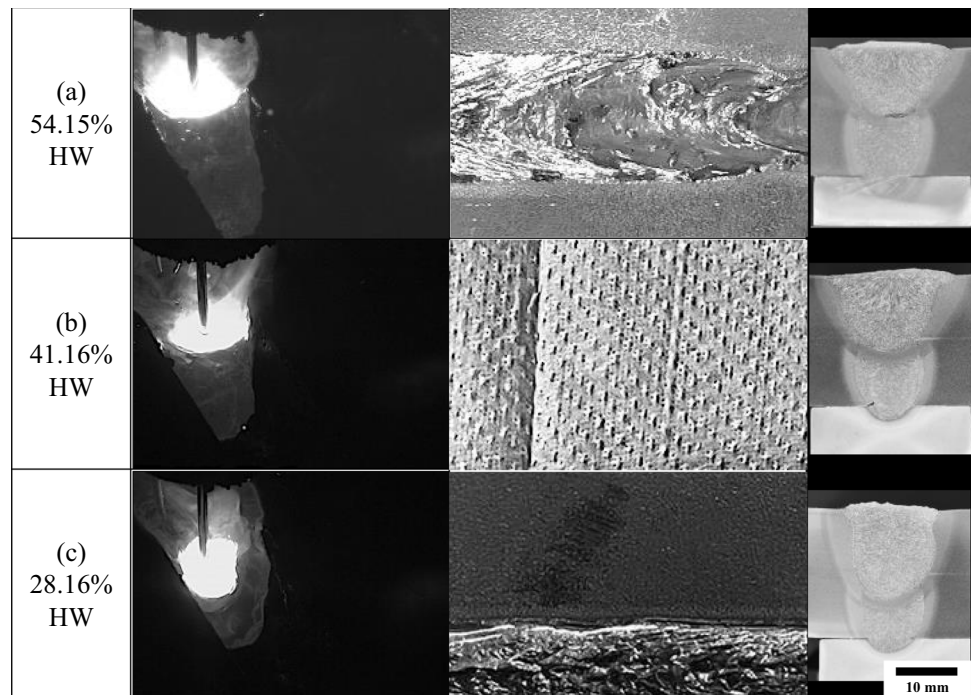


height from the weld cap to the end of the fusion zone in the thickness direction. According to the experimental result, exceeding a hot-wire fraction of 44.05% under a specific deposition rate of 114.95 g/min from GMAW led to the unmelted at the interlayer of the first and second layer of single-V joint of a 20-mm thick steel plate. These parameters were found to optimize the mechanical properties of the weld metal.

In Fig. 12, Vickers hardness tests were conducted on etched surfaces of the weld metal areas, as indicated by the blue bars. The results showed a consistent pattern of hardness values, ranging from 191 ± 10 to 192 ± 11 HV10, within the hot-wire fractions of 36.18 to 44.05%. However, outside this range, the hardness exhibited a decrease,

ranging from 179 ± 7 to 165 ± 7 HV10 for hot-wire fractions of 49.60% and 54.15%, respectively. The green bars in the figure represent the absorbed impact energy values obtained from Charpy impact tests, and these results demonstrated similarity across hot-wire fractions ranging from 36.18 to 44.05%, with values in the range of 77 ± 5 to 78 ± 5 J. These mechanical properties align consistently with the predominant microstructures discussed earlier in this study. The larger grain sizes of grain boundary ferrite (GBF) and secondary phase ferrite (SPF) observed in these experiments are attributed to slower cooling rates, which occur with excessive hot-wire fractions. These larger grain sizes are associated with reduced impact toughness. It is worth noting that the condition with a 54.15% hot-wire

Fig. 13 Captured arc observations and bead appearances for a 54.15% HW, b 41.16% HW, and c 28.16% HW



fraction could not be tested due to significant issues with incomplete fusion. As a result, the 49.60% hot-wire fraction exhibited the lowest absorbed impact energy among the tested conditions.

3.3 Optimized conditions

As per the findings discussed in the previous section, it is evident that to ensure complete joint filling with only a second layer, the minimum required total deposition rate should be at least 250.72 g/min. However, at these deposition rates, issues of incomplete fusion at the interlayer are encountered. To address this, optimization was focused on the fraction between GMAW and hot-wire while keeping the total deposition rate constant. To address the issue of incomplete fusion and improve penetration, the GMAW fraction was increased, while keeping the total deposition rate constant. During the arc observation, it was noticed that as the GMAW fraction increased, the arc

position shifted downward in the thickness direction. This shift resulted in a reduced accumulation of molten metal at the front of the molten pool, as depicted in Fig. 13. Importantly, this adjustment prevented the occurrence of molten metal precedence. Under the optimized welding condition with a hot-wire fraction of 41.16%, a regular bead shape was achieved.

However, increasing the GMAW fraction led to an increase in the welding current. Energy input was consequently increased and affected the cooling time from 800 to 500 °C. Figures 13a–c illustrate microstructures of the weld metals obtained with hot-wire fractions of 54.15%, 41.16%, and 28.16% of the total deposition rate of 250.72 g/min, respectively. These microstructures showed that without experiencing a lack of fusion, the predominant presence of grain boundary ferrite (GBF) and secondary phase ferrite (SPF) transformed into a predominantly acicular ferrite (AF) even at a slower cooling rate (Fig. 14).

Fig. 14 Cooling rates and weld metal microstructures for **a** 44.05% HW, **b** 49.60% HW, and **c** 54.15% HW

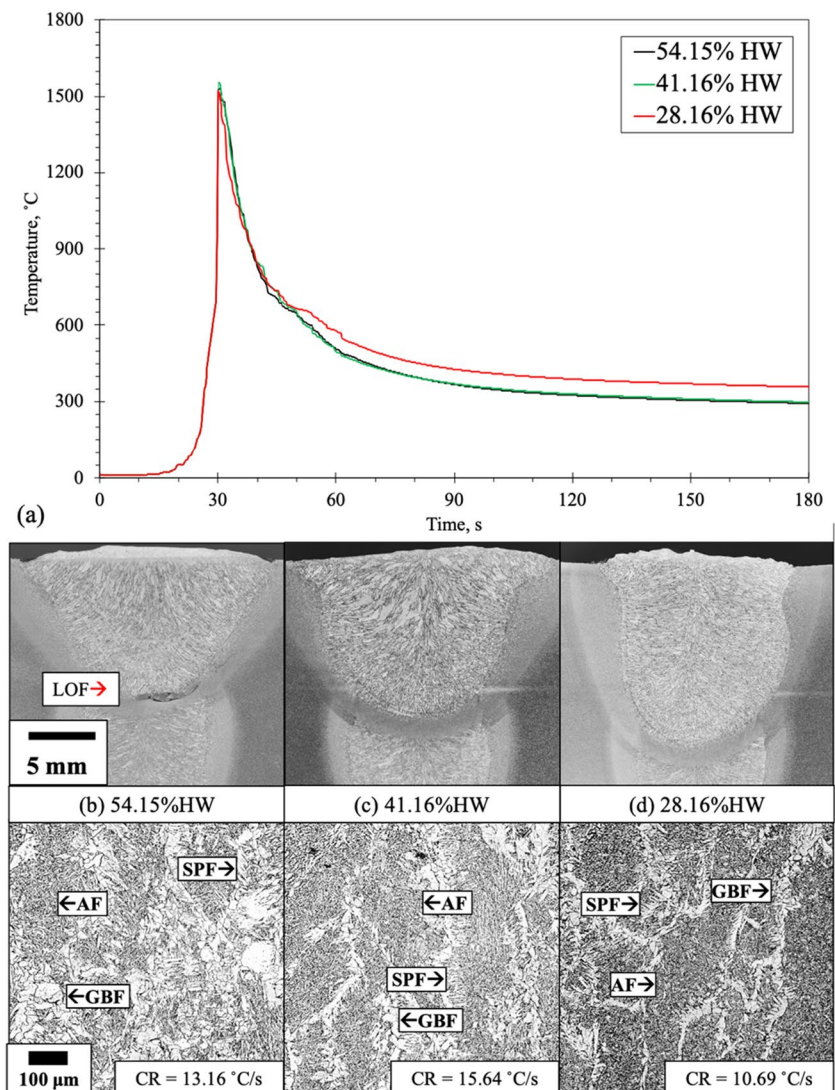


Fig. 15 Weld geometry measurement at hot-wire optimized condition

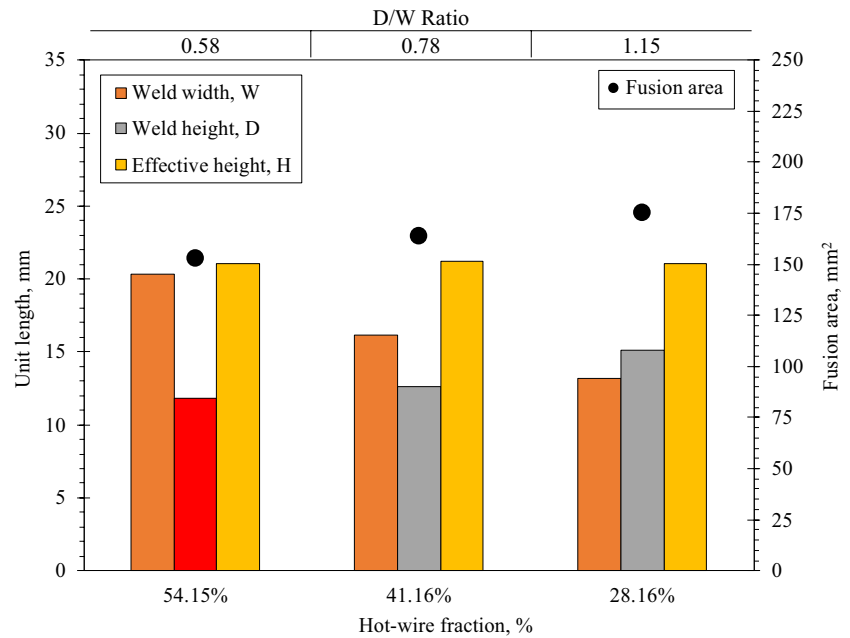
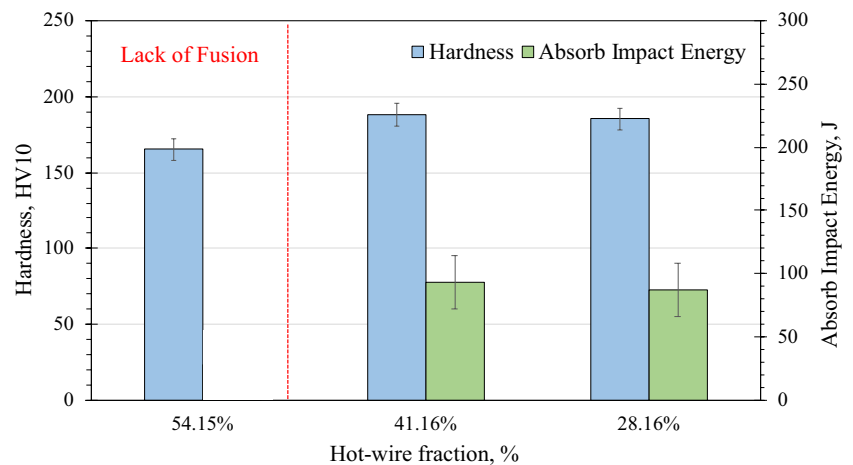


Fig. 16 Hardness and toughness of various hot-wire fractions but similar total deposition rate



All three conditions at a total deposition rate of 250.72 g/min resulted in a similar effective height with reinforcement at the weld cap, as indicated by the yellow bars in Fig. 15. Furthermore, reducing the hot-wire fraction while keeping the total deposition rate constant resulted in a narrower weld width and higher weld height compared to the original hot-wire fraction of 54.15%. This adjustment increased the obtained D/W ratio and fusion area. Optimizing the balance between GMAW and hot-wire not only achieved the desired deposition rate but also influenced the shape and position of the weld metal in the thickness direction.

The optimized ratio between hot-wire and GMAW fractions yielded significant improvements in hardness and absorb impact energy. Figure 16 demonstrates that a

hot-wire fraction of 41.16% resulted in enhanced absorb impact energy, indicated by the green bars. (Hardness value increased from 165 ± 7 to 191 ± 7 HV10 and absorb impact energy increased to 72 ± 7 J.) The power consumption for GMAW alone, providing a deposition rate of 250.72 g/min, is shown by the black bar in Fig. 17. Power consumptions for the three optimized conditions are presented. The condition with 54.15% hot-wire fraction, which led to a lack of fusion, is represented by the red bar. Notably, the 41.16% hot-wire fraction exhibited the lowest power consumption, with an approximate 62% reduction compared with GMAW alone at a similar deposition rate. These findings identify the best-optimized condition for achieving a sound 20-mm single-V butt joint, accompanied by a substantial 62% reduction

Fig. 17 Relationship between power consumption and hot-wire fraction at optimized conditions

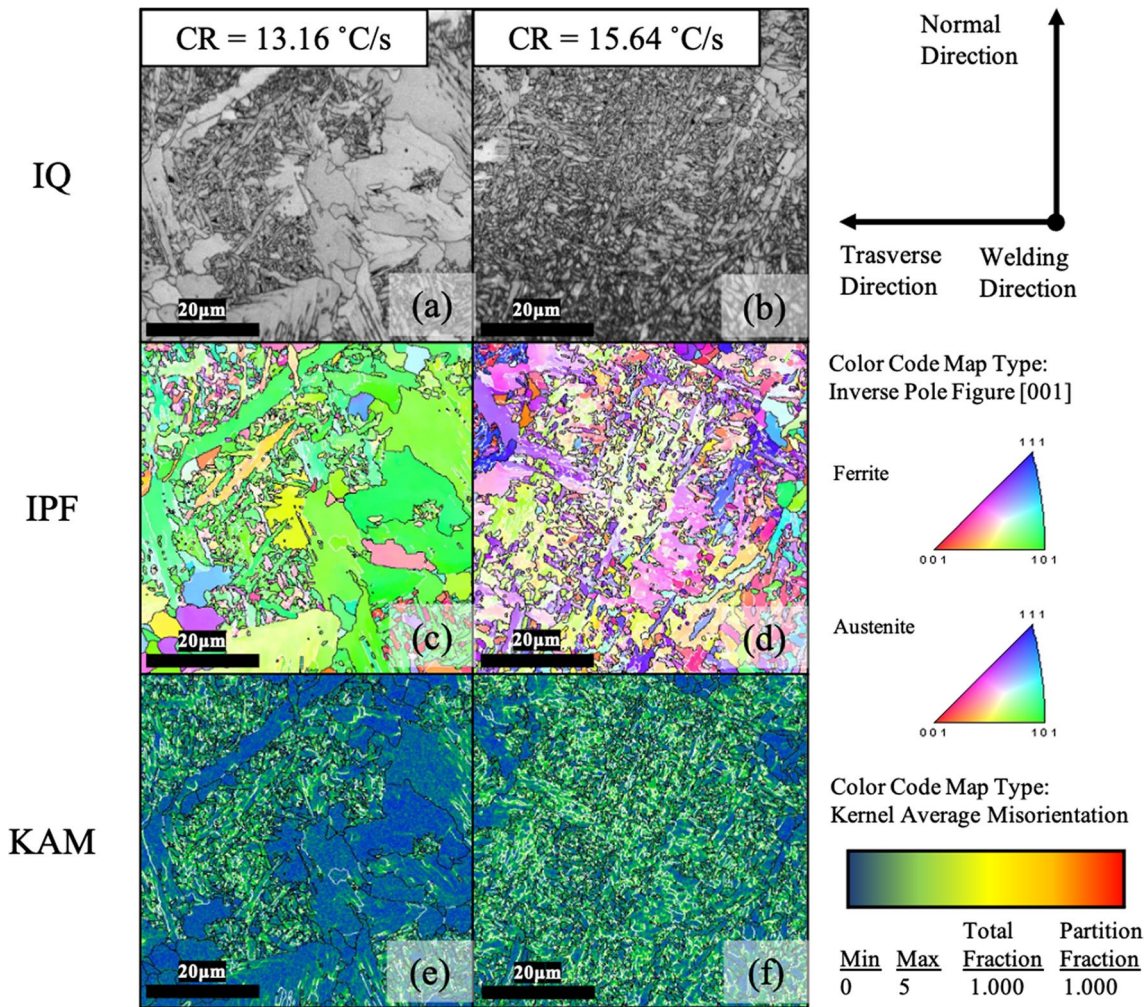
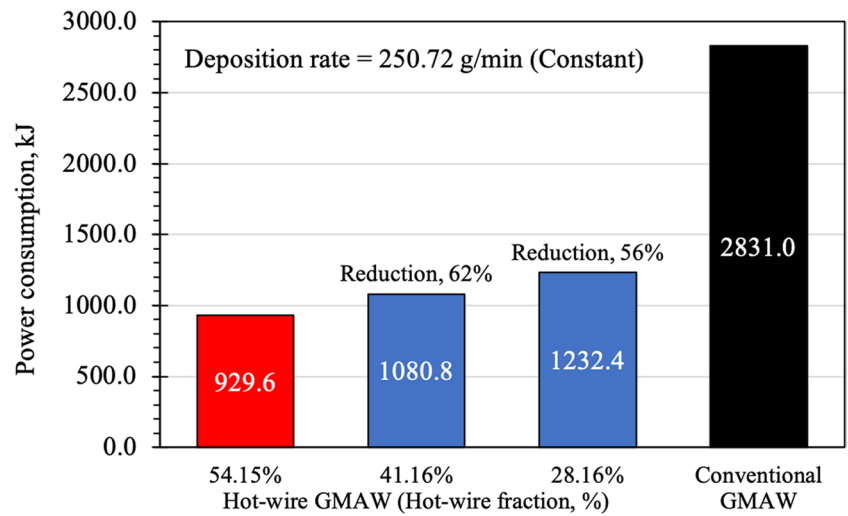


Fig. 18 Comparison of EBSD results: IQ maps a and b; IPF maps c and d; KAM maps e and f

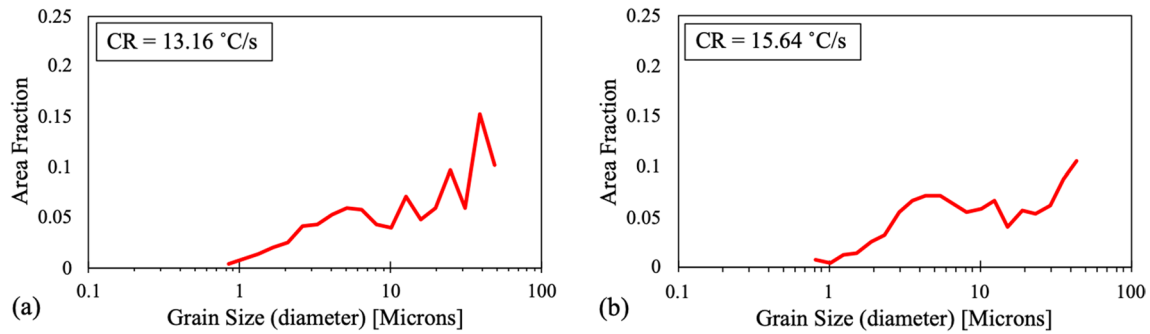


Fig. 19 Average grain size fraction from weld metal produced from **a** 54.15% hot-wire and **b** 41.16% hot-wire

in power consumption, while maintaining desired joint properties.

For further insight and emphasis on the condition with the lowest energy consumption, EBSD analysis was conducted on the weld metal samples. The analysis compared the weld metals produced with hot-wire fractions of 54.15% and 41.16%. The EBSD image quality maps revealed a mixture of ferrite morphologies. The predominantly GBF and SPF in the weld metal with a 54.15% hot-wire fraction, as shown in Fig. 18a, transformed into predominantly AF in the weld metal with a 41.16% hot-wire fraction, as seen in Fig. 18b. The image pole figure maps displayed a greater variety of AF orientations and an increased total grain boundary length, indicating improved resistance to deformation and crack propagation, leading to enhanced mechanical properties. The kernel-average misorientation (KAM) maps in Fig. 18e and f show a higher dislocation density in the AF region, attributed to the unique needle-like morphology of AF.

Figure 19 illustrates the average grain size fraction, revealing that the weld metal produced with a 41.16% hot-wire fraction exhibited a larger proportion of smaller grain sizes compared to the weld metal with a 54.15% hot-wire fraction. The misorientation angle profile, detailed in Fig. 20, revealed distinctive differences between these two conditions. Notably, a substantial

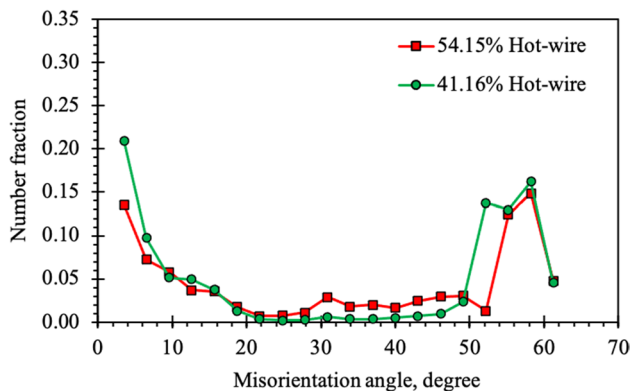


Fig. 20 Average misorientation angle of weld metal produced from **a** 54.15% hot-wire; **(b)** 41.16% hot-wire

fraction of misorientation angles, primarily at 50 and 60°, was observed [36, 38, 39]. This suggests the presence of mixed polygonal ferrite with AF in the weld metal area [36, 38, 39, 40].

4 Conclusion

This comprehensive investigation systematically explored the influence of hot-wire fraction on a 20-mm thick steel plate butt joint. Utilizing high-speed camera technology for real-time monitoring, the study unveiled crucial insights into the welding process. The conclusions drawn from this study are as follows:

- (1) Hot-wire insertion improves weld metal properties and can compensate for the desired deposition rate compared with conventional GMAW.
- (2) Motion analysis using a high-speed camera identified molten metal precedence, which can be avoided with the use of an appropriate deposition rate.
- (3) The optimized condition between GMAW and HW fraction provided a sound joint with improved mechanical properties using 250.72 g/min deposition rate with 41.16% of hot-wire fraction.
- (4) The optimized condition for 20-mm thick steel plates enabled the creation of sound joints with only two weld passes, accompanied by a substantial 62% reduction in power consumption compared with traditional GMAW.
- (5) The EBSD analysis highlighted the optimized condition with a 41.16% hot-wire fraction, which not only ensured joint soundness but also resulted in a predominantly acicular ferrite, contributing to higher mechanical properties.

Author contribution All authors contributed to the study conception and design. Material preparation, data collection, and analysis were

performed by NS, MY, and SS. The first draft of the manuscript was written by NS, and all authors commented on previous versions of the manuscript. All authors read and approved the final manuscript.

Data Availability The data that support the findings of this study are available from the corresponding author, Nattasak Suwannatee, upon reasonable request.

Declarations

Conflict of interest The authors declare no competing interests.

References

- Wu Y, Yuan X, Kaldre I, Zhong M, Wang Z, Wang C (2023) TiO₂-assisted microstructural variations in the weld metal of EH36 shipbuilding steel subject to high heat input submerged arc welding. *Metall Mater Trans B* 54:50–55. <https://doi.org/10.1007/s11663-022-02697-x>
- Abe Y, Fujimoto T, Nakatani M, Shigeta M, Tanaka M (2020) Development of a welding condition optimization program for narrow gap SAW. *Q J Jpn* 38(2):98s–102s. <https://doi.org/10.2207/qjws.38.98s>
- Coetsee T, De Bruin FJ (2022) Improved titanium transfer in submerged arc welding of carbon steel through aluminum addition. *Miner Process Extr Metall Rev* 43(6):771–774. <https://doi.org/10.1080/08827508.2021.1945595>
- Donizete Borba TM, Duarte Flores W, de Oliveira TL, Cardoso Junior R (2017) Assessment of the weldability of EH36 TMCP shipbuilding steel welded by high heat input submerged arc welding. *Weld Int* 31(3):184–195. <https://doi.org/10.1080/09507116.2016.1218619>
- Chen Y, Fang C, Yang Z, Wang J, Wu M, Chen S (2017) A study on sidewall penetration of cable-type welding wire electro-gas welding. *Weld World* 61:979–986. <https://doi.org/10.1007/s40194-017-0479-0>
- Liu F, Tao C, Dong Z, Jiang K, Zhou S, Zhang Z, Shen C (2021) Prediction of welding residual stress and deformation in electro-gas welding using artificial neural network. *Mater Today Commun* 29:102786. <https://doi.org/10.1016/j.mtcomm.2021.102786>
- Fu J, Tao Q, Yang X, Nenchev B, Li M, Tao B, Dong H (2022) The effect of heat source path on thermal evaluation during electro-gas welding of thick steel plates. *Materials* 15(6):2215. <https://doi.org/10.3390/ma15062215>
- Feng J, Guo W, Francis J, Irvine N, Li L (2016) Narrow gap laser welding for potential nuclear pressure vessel manufacture. *J Laser Appl* 28(2):022421. <https://doi.org/10.2351/1.4943905>
- Roland F, Manzon L, Kujala P, Brede M, Weitzenbock J (2004) Advanced joining techniques in European shipbuilding. *J Ship Prod* 20(03):200–210. <https://doi.org/10.5957/jsp.2004.20.3.200>
- Elmer JW, Vaja J, Gibbs G (2022) Reduced pressure laser weld comparison to electron beam welds in Ti-6Al-4 V. *Weld World* 66:2053–2071. <https://doi.org/10.1007/s40194-022-01356-8>
- Feng G, Wang Y, Luo W, Hu L, Deng D (2021) Comparison of welding residual stress and deformation induced by local vacuum electron beam welding and metal active gas arc welding in a stainless steel thick-plate joint. *J Mater Res Technol* 13:1967–1979. <https://doi.org/10.1016/j.jmrt.2021.05.105>
- Acherjee B (2018) Hybrid laser arc welding: state-of-art review. *Opt Laser Technol* 99:67–71. <https://doi.org/10.1016/j.optlastec.2017.09.038>
- Marumoto K, Tamata H, Fujinaga A, Takahashi T, Yamamoto H, Choi J, Yamamoto M (2023) Bead shape control in high-speed fillet welding using hot-wire GMA laser hybrid welding technology. *Weld World* 67(5):1259–1266. <https://doi.org/10.1007/s40194-023-01496-5>
- Reisgen U, Olschok S, Jakobs S, Schleser M, Mokrov O, Rossiter E (2012) Laser beam submerged arc hybrid welding. *Phys Procedia* 39:75–83. <https://doi.org/10.1016/j.phpro.2012.10.016>
- Reisgen U, Olschok S, Jakobs S, Engels O (2016) Modern hybrid welding process for structural steelwork engineering - laser submerged arc hybrid welding. *J Laser Appl* 28:022011. <https://doi.org/10.2351/1.4944112>
- Júnior RC, Esteves L, Santos NF, Oliveira IR, Mendes DS, Lins VFC, Modenesi PJ (2019) Influence of heat input and cold wire feeding rate on pitting corrosion resistance of submerged arc welding duplex stainless steel welds. *J Mater Eng and Perform* 28:1969–1976. <https://doi.org/10.1007/s11665-019-03967-7>
- Xiang T, Li H, Wei HL, Gao Y (2016) Arc characteristics and metal transfer behavior of twin-arc integrated cold wire hybrid welding. *Int J Adv Manuf Technol* 87:2653–2663. <https://doi.org/10.1007/s00170-016-8663-8>
- Xiang T, Li H, Huang CQ, Wei HL, Li JX, Gao Y (2017) The metal transfer behavior and the effect of arcing mode on metal transfer process in twin-arc integrated cold wire hybrid welding. *Int J Adv Manuf Technol* 90:1043–1050. <https://doi.org/10.1007/s00170-016-9451-1>
- Holliday DB, Dull RM, Hartman DK, Wright DA (2004) Chapter 4-gas metal arc welding. In: *Welding A (ed) Welding Handbook Volume 2, 9th. Society, Miami, FL*, pp 1488–2197
- Shinozaki K, Yamamoto M, Mitsuhashi K, Nagashima T, Kanazawa T, Arashin H (2011) Bead formation and wire temperature distribution during ULTRA-HIGH-SPEED GTA WELDING using pulse-heated hot-wire. *Weld World* 55(3–4):12–18. <https://doi.org/10.1007/2FBF03321281>
- Zhu S, Nakahara Y, Yamamoto M (2021) Optimization of process conditions for additive manufacturing technology combining high-power diode laser and hot wire. *Metals* 11:1583. <https://doi.org/10.3390/met11101583>
- Liu W, Liu S, Ma J, Kovacevic R (2014) Real-time monitoring of the laser hot-wire welding process. *Opt laser Technol* 57:66–76. <https://doi.org/10.1016/j.optlastec.2013.09.026>
- Li J, Sun Q, Kang K, Zhen Z, Liu Y, Feng J (2020) Process stability and parameters optimization of narrow-gap laser vertical welding with hot wire for thick stainless steel in nuclear power plant. *Opt laser Technol* 123:105921. <https://doi.org/10.1016/j.optlastec.2019.105921>
- Metzbower EA, Bhadeshia HKDH, Phillips RH (1994) Microstructure in hot-wire laser beam welding of HY 80 steel. *Mater Sci Technol* 10(1):56–59. <https://doi.org/10.1179/mst.1994.10.1.56>
- Tsuyama T, Nakai K, Tsuji T (2014) Development of submerged arc welding method using hot wire. *Weld World* 58:713–718. <https://doi.org/10.1007/2Fs40194-014-0153-8>
- Tsuyama T, Yuda M, Nakai K (2014) Effect of hot wire on mechanical properties of weld metal using gas-shielded arc welding with CO₂ gas. *Weld World* 58:77–83. <https://doi.org/10.1007/2Fs40194-013-0094-7>
- Suwannatee N, Yamamoto M (2023) Single-pass of square butt joints without edge preparation using hot-wire gas metal arc welding. *Metals* 13(6):1014. <https://doi.org/10.3390/met13061014>
- Wonthaisong S, Shinohara S, Shinozaki K, Phaoniam R, Yamamoto M (2021) Evaluation of butt joint produce by a hot-wire CO₂ arc welding method. *Q J Jpn* 39(1):96–103. <https://doi.org/10.2207/qjws.39.96>
- Suwannatee N, Wonthaisong S, Yamamoto M, Shinohara S, Phaoniam R (2021) Optimization of welding conditions for hot-wire

- GMAW with CO₂ shielding on heavy-thick butt joint. *Weld World* 66:833–844. <https://doi.org/10.1007/s40194-021-01227-8>
30. Kou S (2003) Work-hardened materials. In *Welding metallurgy* 2nd ed. John Wiley & Sons, Inc, Hoboken, NJ, USA, pp 343–351
 31. Chen H, Yang Z, Zhang C, Zhu K, van der Zwaag S (2016) On the transition between grain boundary ferrite and bainitic ferrite in Fe-C-Mo and Fe-C-Mn alloys: the bay formation explained. *Acta Mater* 104:62–71. <https://doi.org/10.1016/j.actamat.2015.11.012>
 32. Jia X, Yang Y, Ma Y, Wang B, Wang B (2023) In situ observation of phase transformations in the partially melted zone of HSLA offshore steel during simulated welding process. *Mater Today Commun* 34:105012. <https://doi.org/10.1016/j.mtcomm.2022.105012>
 33. Wu HD, Miyamoto G, Yang Z, Zhang C, Chen H, Furuhashi T (2018) Carbon enrichment during ferrite transformation in Fe-Si-C alloys. *Acta Mater* 149:68–77. <https://doi.org/10.1016/j.actamat.2018.02.040>
 34. Babu SS (2004) The mechanism of acicular ferrite in weld deposits. *Curr Opin Solid State Mater Sci* 8(3–4):267–278. <https://doi.org/10.1016/j.cossms.2004.10.001>
 35. Shao Y, Liu C, Yan Z, Li H, Liu Y (2018) Formation mechanism and control methods of acicular ferrite in HSLA steel: a review. *J Mater Sci Technol* 34(5):737–744. <https://doi.org/10.1016/j.jmst.2017.11.020>
 36. Jorge JCF, De Souza LFG, Mendes MC, Bott IS, Araújo LS, Dos Santos VR, Rebello JMA, Evans GM (2021) Microstructure characterization and its relationship with impact toughness of C-Mn and high strength low alloy steel weld metals—a review. *J Mater Res Technol* 10:471–501. <https://doi.org/10.1016/j.jmrt.2020.12.006>
 37. Cho L, Tselikova A, Holtgrewe K, De Moor E, Schmidt R, Findley KO (2022) Critical assessment 42: acicular ferrite formation and its influence on weld metal and heat-affected zone properties of steels. *Mater Sci Technol* 38(17):1425–1433. <https://doi.org/10.1080/02670836.2022.2088163>
 38. Gourgues AF, Flower HM, Lindley TC (2000) Electron backscattering diffraction study of acicular ferrite, bainite, and martensite steel microstructures. *Mater Sci Technol* 16(1):26–40. <https://doi.org/10.1179/026708300773002636>
 39. Shrestha SL, Breen AJ, Trimby P, Proust G, Ringer SP, Cairney JM (2014) An automated method of quantifying ferrite microstructures using electron backscatter diffraction (EBSD) data. *Ultramicroscopy* 137:40–47. <https://doi.org/10.1016/j.ultramic.2013.11.003>
 40. Diaz-Fuentes M, Iza-Mendia A, Gutierrez I (2003) Analysis of different acicular ferrite microstructures in low-carbon steels by electron backscattered diffraction. Study of their toughness behavior. *Metall Mater Trans A* 34:2505–2516. <https://doi.org/10.1007/s11661-003-0010-7>

Publisher's Note Springer Nature remains neutral with regard to jurisdictional claims in published maps and institutional affiliations.

Springer Nature or its licensor (e.g. a society or other partner) holds exclusive rights to this article under a publishing agreement with the author(s) or other rightsholder(s); author self-archiving of the accepted manuscript version of this article is solely governed by the terms of such publishing agreement and applicable law.